Low-energy positronium scattering from O$_2$

D. M. Newson, R. Kadokura, H. Allen, S. E. Fayer, S. J. Brawley, M. Shipman, and G. Laricchia[*]

Department of Physics and Astronomy, University College London, Gower Street, London WC1E 6BT, United Kingdom

R. S. Wilde

Department of Natural Sciences, Oregon Institute of Technology, Klamath Falls, Oregon 97601, USA

I. I. Fabrikant

Department of Physics and Astronomy, University of Nebraska, Lincoln, Nebraska 68588-0299, USA

L. Sarkadi

ATOMKI, Institute for Nuclear Research, H-4026 Debrecen, Bem ter 18/c, Hungary

The total cross section of positronium (Ps) scattering from molecular oxygen has been measured in the velocity range 0.27–1.50 a.u. (energy range 2–61 eV) and has been found to be close to the corresponding equivelocity electron cross section above 0.87 a.u. (20 eV), as previously found by Brawley *et al.*, [Science **330**, 789 (2010)]. However, below this value the cross section for positronium is observed to exceed that for electrons by up to a factor of 4 at the lowest energy. Measurements are compared to the predictions of low-energy resonant peaks in the elastic-scattering cross section calculated within a free-electron-gas model refined by applying corrections to the correlation energy for the interaction between Ps and the electron gas. Additionally, cross sections for O$_2^-$ formation and positronium breakup have been calculated using a classical-trajectory Monte Carlo approach. Comparisons are made with earlier calculations and discussed in terms of both experimental and theoretical uncertainties.

I. INTRODUCTION

Positronium (Ps) is a hydrogenic atom consisting of an electron (e^-) and a positron (e^+). It is metastable against annihilation with lifetimes of 125 ps and 142 ns for the 1^1S_0 and 1^3S_1 states, respectively [1]. The purely leptonic nature of Ps makes it an ideal subject for testing predictions of quantum electrodynamics [2,3], and its light mass and neutrality render it an interesting projectile, especially when compared with e^+, e^-, ions, and other atoms [4,5]. In particular, the overall probability of Ps scattering from a wide variety of atoms and molecules has been observed to be similar to that of equivelocity electrons [6], even in the vicinity of delicate quantum-mechanical effects, such as resonances in CO$_2$ and N$_2$ [7–10].

However, the similarity has been predicted usually to disappear in the low-energy region, although the size of this region depends on the target: for rare-gas atoms this similarity is observed immediately above the Ps breakup threshold ($E_{Ps} = 6.8$ eV or $v_{Ps} \simeq 0.5$ a.u.) [11], whereas for molecules the merging of electron and Ps total cross sections occurs at

higher velocities and for strongly polar molecules the similarity disappears completely [12].

These trends may be understood qualitatively in terms of the basic interactions at play. At intermediate projectile energies, both electron scattering and Ps scattering are essentially controlled by electron exchange, which results in their similarity. On the other hand at low energies, scattering is controlled by a balance of exchange and long-range interaction. The latter is different for electron scattering, where it appears as the polarization force, and Ps scattering, where it appears as the van der Waals force. The result of this balance depends on the target. For nonpolar and weakly polar targets, the low-energy Ps-scattering cross section might be below that for electrons, for example, in the case of H$_2$ [13], but also can exceed it, which is apparent in collisions with N$_2$ [9]. For highly polar targets, the electron-scattering cross section is always larger because of the strong electron-dipole interaction [12].

The O$_2$ molecule is of special interest, particularly from the point of view of resonance scattering. While for N$_2$ and CO$_2$, low-energy resonances were observed [7,8] and confirmed by calculations for both electron and Ps scattering [9,10], the low-energy $^2\Pi_g$ resonance in e^--O$_2$ scattering is extremely narrow [14,15] and was observed only in experiments with high-energy resolution [16,17]. Since its width is smaller than the vibrational spacing in O$_2$, the resonance appears as a series of peaks near the vibrational excitation thresholds [17]; therefore, for their theoretical description one has to go beyond the fixed-nuclei approximation. In contrast, calculations of

---

[*]g.laricchia@ucl.ac.uk

Ps-O_2 scattering in the fixed-nuclei approximation [10] show that there are two broader low-velocity peaks in the elastic-scattering cross section due to a combination of resonances of different symmetries.

Experimentally, studies of Ps scattering at low energies are challenging due to the inherently weak Ps beam intensities arising from the combination of poor efficiencies for the production of Ps, its survival against in-flight annihilation, and its detection [18], as well as the possible occurrence of minima in the differential Ps-formation cross sections at small forward angles, potentially linked to quantum vortices at larger angles [19–21]. In the present study, measurements of the Ps-O_2 total-scattering cross section Q_T^{Ps} have been extended to below the Ps breakup threshold to investigate possible deviations from electronlike behavior [6] and explore the recent prediction of resonant peaks at approximately 2 and 4 eV [10].

The latter was based on calculations employing the free-electron-gas (FEG) model for electron exchange and correlations in Ps collisions with neutral targets [22]. This model has certain limitations, the most severe of which is the approximation of the plane-wave Thomas-Fermi model for target electrons. Other issues are discussed in the present work, and a more accurate inclusion of correlation energy is given in Sec. III. Additionally, the cross sections for O_2^- formation and positronium breakup have been calculated using a classical-trajectory Monte Carlo (CTMC) approach. Comparisons are made with earlier calculations and discussed in terms of both experimental and theoretical uncertainties.

II. EXPERIMENTAL APPARATUS AND METHOD

Q_T^{Ps} has been measured using the Ps beamline at UCL, described elsewhere (e.g., [23]). Only some key features are summarized here. A β^+ emitter (^{22}Na) is used in conjunction with a solid Ne moderator to produce slow positrons (energy distribution FWHM $\simeq 1$ eV), confined radially by a magnetic field of $\sim 10^{-2}$ T and accelerated by a positive voltage applied to the source. After deflection by an $\mathbf{E} \times \mathbf{B}$ filter and transmission through several collimators, the e^+ beam traverses a gas cell, where it may collide with a suitable gas (A) to produce forward-going Ps via charge exchange (e.g., [24,25]),

$$e^+ + A \rightarrow Ps + A^+. \tag{1}$$
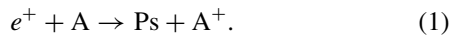
Ps is detected by impact upon a channel electron multiplier (CEM; Dr. Sjuts KBL25RS/90) [18] in coincidence with the registration of an annihilation γ ray by one of two scintillator detectors (NaI or CsI).

The Ps energy E_{Ps} and its distribution ΔE_{Ps} are primarily determined by that of the incident e^+ beam. The former is given by

$$E_{Ps} \simeq E_+ - E_I + \frac{6.8 \text{ eV}}{n^2}, \tag{2}$$

where E_+ is the energy of the incoming e^+ beam, E_I is the first ionization energy of the production gas (in this case, 15.76 eV for Ar), and n is the Ps principal quantum number, dominantly $n = 1$ [26,27].

The total cross section is determined by measuring the incident and transmitted Ps beam intensities I_0 and I (both net of their respective backgrounds) emerging from a second gas
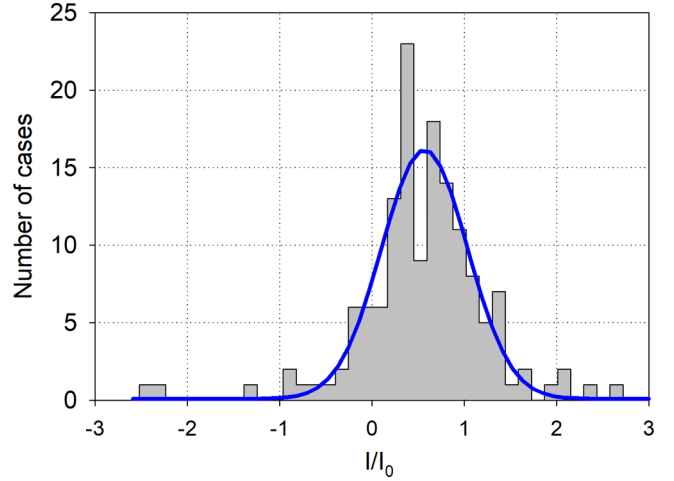

FIG. 1. Histogram of I/I_0 for $E_{Ps} = 2$ eV and the Gaussian fit to the data ($R^2 \sim 0.9$).

cell and applying the Beer-Lambert law:

$$Q_T^{Ps} = -\frac{k_B T}{p l_{eff}} \ln \left(\frac{I}{I_0} \right), \tag{3}$$

where l_{eff} is the effective length of the cell (59.2 ± 0.1 mm), p is the pressure of the scattering gas, k_B is the Boltzmann constant, and T is the ambient temperature. The pencil angle of the Ps beam is $\simeq 1.2°$, set by the radius (3 mm) of the exit aperture of the scattering cell and its distance from the center of the Ps formation cell (147.6 mm). The angular discrimination against forward-scattered particles is $\simeq 2.3°$, determined by the radius (12.5 mm) of the CEM and its position relative to the center of the scattering cell (311.2 mm).

At each E_{Ps}, the pressure was set such that $I/I_0 \simeq 50\%$, although fluctuations in count rates, gas pressure, and detector noise result in a distribution of I/I_0, as illustrated in Fig. 1 for $E_{Ps} = 2$ eV, the lowest energy investigated. In order to discriminate against the effects of large fluctuations, which have been found to be significant at low energies ($\leqslant 5$ eV), Q_T^{Ps} has been determined from measurements with $0 < I/I_0 < 1$ [28,29], consistent with the FWHM of a Gaussian fit to the data, also shown in Fig. 1. The ensuing cross sections were classified into groups first according to E_{Ps} (± 0.5 eV centered on integers) and then by the average incident e^+ beam intensity (± 5 kHz centered on multiples of 10 kHz), recorded before and after each Ps beam-attenuation measurement. In this way, measurements were categorized according to their experimental conditions, and the arithmetic mean $\langle Q_T^{Ps} \rangle$ and standard error were computed for each group. The final Q_T^{Ps} was hence obtained as the weighted average of the $\langle Q_T^{Ps} \rangle$ values.

III. THEORETICAL METHODS

A. FEG model with exchange-correlation term: Elastic-scattering cross section

The method of inclusion of exchange and correlations in Ps-neutral target scattering was developed in Ref. [22] and applied to several molecular targets [9,10,12]. The FEG potential does not include the Pauli exclusion principle completely

since it does not prevent e^- capture in an occupied orbital of the target. In addition, the exchange and correlation energies for this model were calculated in the first nonvanishing order of the perturbation theory: the first order in Ps-target interaction for exchange and the second order for correlations. An additional approximation was also made by neglecting the exchange contribution to the correlation term. To check the reliability of the latter approximation, it is improved in the present study by inclusion of the interference term in the correlation energy. The error due to the incomplete inclusion of the Pauli exclusion principle will be discussed in Sec. IV.

Using atomic units, the second-order correction to Ps energy due to interaction with an electron in the Fermi gas is, according to Eq. (13) of [22],

$$E_{1\mathbf{pk}m_1m_2}^{(2)} = \sum_{nlm\mathbf{p'k'}m_1'm_2'} \frac{|\langle nlm\mathbf{p'k'}|H'|100\mathbf{pk}\rangle|^2}{E_{1\mathbf{pk}} - E_{n\mathbf{p'k'}} + i\eta}, \qquad (4)$$

where H' is the Ps-electron interaction and

$$E_{npk} = \epsilon_n + \mathbf{p}^2/4 + \mathbf{k}^2/2 \qquad (5)$$

is the total energy of the system of a free e^- with momentum $\mathbf{k}$ and Ps with momentum $\mathbf{p}$ and binding energy ϵ_n, nlm are Ps quantum numbers, and m_1 and m_2 are spin quantum numbers of e^- in the gas and Ps, respectively. The total correlation energy is

$$E_{1\mathbf{p}}^{\mathrm{corr}} = \sum_{km_1} E_{1\mathbf{pk}m_1m_2}^{(2)}. \qquad (6)$$

The matrix element $\langle nlm\mathbf{p'k'}|H'|100\mathbf{pk}\rangle$ can be separated into the direct term M_{dir} and the exchange term M_{ex}. The first has been used previously (Eq. (14) in Ref. [22]) and can be written as

$$M_{\mathrm{dir}} = \frac{\delta_{m_1m_1'}\delta_{m_2m_2'}}{V^2} \int e^{i\mathbf{R}_1\cdot\mathbf{Q}} e^{i\mathbf{r}_2\cdot\mathbf{q}} \psi_{nlm}^*(\boldsymbol{\rho}_1)\psi_{100}(\boldsymbol{\rho}_1)$$

$$\times \left(\frac{1}{r_{12}} - \frac{1}{r_{2p}}\right) d\mathbf{r}_1 d\mathbf{r}_2 d\mathbf{r}_p, \qquad (7)$$

where V is the normalization volume, $\mathbf{r}_1$ and $\mathbf{r}_2$ are e^- position vectors, $\mathbf{r}_p$ is the e^+ position vector, $\mathbf{R}_i = (\mathbf{r}_i + \mathbf{r}_p)/2$, $i = 1, 2$, $\boldsymbol{\rho}_1 = \mathbf{r}_1 - \mathbf{r}_p$, $\mathbf{Q} = \mathbf{p} - \mathbf{p'}$, and $\mathbf{q} = \mathbf{k} - \mathbf{k'}$. For the exchange contribution, the following is obtained:

$$M_{\mathrm{ex}} = -\frac{\delta_{m_1'm_2}\delta_{m_2'm_1}}{V^2} \int e^{-i\mathbf{k'}\cdot\mathbf{r}_1 - i\mathbf{p'}\cdot\mathbf{R}_2} \psi_{nlm}^*(\boldsymbol{\rho}_2)\psi_{100}(\boldsymbol{\rho}_1)$$

$$\times \left(\frac{1}{r_{12}} - \frac{1}{r_{2p}}\right) e^{i\mathbf{k}\cdot\mathbf{r}_2 + i\mathbf{p}\cdot\mathbf{R}_1} d\mathbf{r}_1 d\mathbf{r}_2 d\mathbf{r}_p. \qquad (8)$$

Previous investigations [30] suggested that the exchange contribution to correlation energy should be small compared to the direct contribution. Noting this, the term $|M_{\mathrm{ex}}|^2$ will be neglected, concentrating instead on the interference term, whose numerator is given by

$$2\sum_{m_1m_1'm_2'} \mathrm{Re}(M_{\mathrm{dir}}^* M_{\mathrm{ex}}) = 2\mathrm{Re}(\tilde{M}_{\mathrm{dir}}^* \tilde{M}_{\mathrm{ex}}), \qquad (9)$$

where $\tilde{M}_{\mathrm{dir}}$ and $\tilde{M}_{\mathrm{ex}}$ are matrix elements in which dependence on spin quantum numbers has been summed off. Therefore,

the interference contribution to the correlation energy is

$$E_{1\mathbf{p}}^{(\mathrm{int})} = \sum_{nlm\mathbf{p'k'k}} \frac{2\mathrm{Re}(\tilde{M}_{\mathrm{dir}}^* \tilde{M}_{\mathrm{ex}})}{E_{1\mathbf{pk}} - E_{n\mathbf{p'k'}} + i\eta}, \qquad (10)$$

with the restriction $k < k_F$, $k' > k_F$.

Changing the integration variables to

$$\boldsymbol{\rho}_1 = \mathbf{r}_1 - \boldsymbol{r}_p, \quad \boldsymbol{\rho}_2 = \mathbf{r}_2 - \boldsymbol{r}_p, \quad \mathbf{r}_p' = \mathbf{r}_p, \qquad (11)$$

the following is obtained:

$$\tilde{M}_{\mathrm{ex}} = -\frac{\delta_{\mathbf{p}+\mathbf{k},\,\mathbf{p'}+\mathbf{k'}}}{V} \int e^{i\boldsymbol{\rho}_1\cdot(\mathbf{p}/2-\mathbf{k'}) - i\boldsymbol{\rho}_2\cdot(\mathbf{p'}/2-\mathbf{k})}$$

$$\times \psi_{nlm}^*(\boldsymbol{\rho}_2)\psi_{100}(\boldsymbol{\rho}_1)\left(\frac{1}{\rho_{12}} - \frac{1}{\rho_2}\right) d\boldsymbol{\rho}_1 d\boldsymbol{\rho}_2, \qquad (12)$$

where the Kronecker delta in front represents the conservation of momentum, which can be rewritten as

$$\mathbf{k} - \mathbf{k'} = \mathbf{p'} - \mathbf{p} \equiv \mathbf{q}. \qquad (13)$$

Integration can be simplified by going into the momentum space,

$$\psi_{nlm}(\boldsymbol{\rho}) = \frac{1}{(2\pi)^{3/2}} \int e^{i\mathbf{s}\cdot\boldsymbol{\rho}} \phi_{nlm}(\mathbf{s}) d\mathbf{s}. \qquad (14)$$

Then,

$$\tilde{M}_{\mathrm{ex}} = -\frac{1}{V(2\pi)^3} \int d\boldsymbol{\rho}_1 d\boldsymbol{\rho}_2 \left(\frac{1}{\rho_{12}} - \frac{1}{\rho_2}\right)$$

$$\times \int d\mathbf{s}_1 d\mathbf{s}_2 e^{i\boldsymbol{\rho}_1\cdot(\mathbf{p}_1+\mathbf{s}_1) - i\boldsymbol{\rho}_2\cdot(\mathbf{p}_2+\mathbf{s}_2)}$$

$$\times \phi_{nlm}^*(\mathbf{s}_2)\phi_{100}(\mathbf{s}_1), \qquad (15)$$

where

$$\mathbf{p}_1 = \mathbf{p}/2 - \mathbf{k'} = \mathbf{p}/2 - \mathbf{k} + \mathbf{q}, \qquad (16)$$

$$\mathbf{p}_2 = \mathbf{p'}/2 - \mathbf{k} = \mathbf{p}/2 - \mathbf{k} + \mathbf{q}/2. \qquad (17)$$

Part of the integration in Eq. (15) can be performed analytically, resulting in a two-dimensional integral in s and θ_s, where θ_s is the spherical angle in the coordinate system with the polar axis along vector $\mathbf{q}$.

To find the interference contribution, it is necessary to find the sum over $\mathbf{p'k'k}$ in Eq. (10). Only two of these three vectors are independent because of the conservation of momentum, Eq. (13). Let us choose them to be $\mathbf{k}$ and $\mathbf{q}$. Replacing summation by integration, it follows that

$$E_{1\mathbf{p}}^{(\mathrm{int})} = \frac{V^2}{(2\pi)^6} \int d\mathbf{k} d\mathbf{q} \,\theta(|\mathbf{k} - \mathbf{q}| - k_F)\theta(k_F - k)$$

$$\times \sum_n \left(-\frac{3}{4}q^2 + \mathbf{q}\cdot(\mathbf{k} - \frac{1}{2}\mathbf{p}) + \epsilon_1 - \epsilon_n\right)^{-1}$$

$$\times \sum_l \mathrm{Re}(\tilde{M}_{\mathrm{dir}}^{(nl)} * \tilde{M}_{\mathrm{ex}}^{(nl)}), \qquad (18)$$

where the Heaviside θ functions take into account the restrictions $k < k_F$ and $k' > k_F$ and the principal value of the integral is taken. Calculations in the range of parameters of interest show that the corresponding domain in the $\mathbf{q}$-$\mathbf{p}$ space never leads to a singularity in the integrand; therefore, the imaginary part of $E_{1\mathbf{p}}^{(\mathrm{int})}$ is zero.

Since the direction of **q** is fixed, integration over $\hat{q}$ can be replaced by the equivalent integration over $\hat{\mathbf{p}}$. The six-dimensional integration in $k, \theta_k, \phi_k, q, \theta_p$, and ϕ_p can be reduced to a five-dimensional integration since the dependence on ϕ_k and ϕ_p is reduced to the dependence on $\chi = \phi_k - \phi_p$, which comes from p_1 and p_2. Finally, the following is obtained:

$$
E_{1\mathbf{p}}^{(\text{int})} = -\frac{2}{\pi^4} \int_0^{2\pi} (2\pi - \chi) d\chi \int_0^{k_F} k^2 dk \sin\theta_k d\theta_k
$$
$$
\times \int q^2 dq \sin\theta_p d\theta_p
$$
$$
\times \theta(|\mathbf{k} - \mathbf{q}| - k_F) \mathcal{F}(k, \theta_k, q, \theta_p, \chi), \quad (19)
$$

where

$$
\mathcal{F}(k, \theta_k, q, \theta_p, \chi)
$$
$$
= \sum_n \left[-\frac{3}{4}q^2 + \mathbf{q} \cdot (\mathbf{k} - \mathbf{p}/2 + \epsilon_1 - \epsilon_n) \right]^{-1}
$$
$$
\times \sum_l \Xi_{nl}(q) \Pi_{nl}(k, \theta_k, q, \theta_p, \chi), \quad (20)
$$

with

$$
\Xi_{nl} = \frac{1}{q^2 (2l+1)! \Gamma(l+3/2)} \left[\frac{\pi (2l+1)(n+l)!}{2nn_r!} \right]^{1/2} \left(\frac{qa_0}{4} \right)^l
$$
$$
\times \sum_{k=0}^{n_r} \frac{(-n_r)_k}{k!(2l+2)_k} \left(\frac{2}{n} \right)^{k+l+3/2} \frac{\Gamma(2l+k+3)}{y^{2l+3+k}}
$$
$$
\times {}_2F_1 \left(l + \frac{k+3}{2}, -\frac{k+1}{2}; l + \frac{3}{2}; z \right), \quad (21)
$$

where

$$
y^2 = \left(1 + \frac{1}{n} \right)^2 + \frac{q^2 a_0^2}{4}, \quad z = \frac{q^2 a_0^2}{4y^2}, \quad (22)
$$

and ${}_2F_1$ is the Gauss hypergeometric function, $n_r = n - l - 1$ is the radial quantum number, $a_0 = 2$ a.u. is the Bohr radius for Ps, and the real function $\Pi_{nl}(\mathbf{k}, \mathbf{p}, q)$ is defined as

$$
\Pi_{nl}(\mathbf{k}, \mathbf{p}, q) = -\frac{V}{4\pi i^l} \tilde{M}_{\text{ex}}(\mathbf{k}, \mathbf{p}, q). \quad (23)
$$

The result of this calculation gives the total correlation energy as a function of the Fermi momentum k_F. Using the relation between k_F and the electron probability density $\rho(r)$, $k_F = (3\pi^2 \rho)^{1/3}$, the correlation energy is given as a function of distance r.

B. Classical-trajectory Monte Carlo approach: Breakup and O_2^- formation cross sections

The CTMC method, as a classical approach, cannot be applied for the calculation of the total-scattering cross section. This is because elastic scattering, as an important contribution to the total cross section, cannot be treated classically: the cross section is infinite even for neutral colliding partners. However, CTMC is suitable for the calculation of the contributions of two significant channels, namely, Ps fragmentation and electron transfer from Ps to the target.

In this work, we used the three-dimensional, three-body version of the CTMC method [31,32]. It is based on a numerical solution of Newton's classical equations of motion for a large number of collision events under randomly chosen initial conditions. The three particles in the present case are e^- and e^+ of Ps and the ground-state O_2 molecule. This approach means that O_2 is considered a structureless, pointlike particle which, however, as a molecule interacts with e^- and e^+ of Ps through an anisotropic potential.

The same calculation procedure was applied in a previous study of the fragmentation of Ps in collision with He atoms [33], except for the treatment of the potential around the target (O_2 instead of He). Therefore, in what follows, the discussion is restricted to only the latter specific feature.

In the past decade, extended CTMC calculations for collisions involving molecular species were carried out [34–36]. In these works the force between a pointlike particle of charge q (in the present case e^- or e^+ of Ps) and the molecule was determined as $-q\nabla_{\mathbf{r}_{ij}} V_{\text{mod}}(\mathbf{r}_{ij})$, where $\mathbf{r}_{ij} = \mathbf{r}_i - \mathbf{r}_j$ is the relative position vector of the particle and the center of the molecule. $V_{\text{mod}}(\mathbf{r})$ is a multicenter *model* potential of the mean electric field created by the nuclei and the electrons of the molecule.

$V_{\text{mod}}(\mathbf{r})$ can be well approximated by the sum of screened atomic potentials. For this purpose one may use the Green-Sellin-Zachor potential deduced from atomic structure calculations [37]:

$$
V^{\text{GSZ}}(r) = \{Z - (N-1)[1 - \Omega(r, \eta, \xi)]\}/r, \quad (24)
$$

where Z is the nuclear charge, N is the number of electrons in the ion, and

$$
\Omega(r, \eta, \xi) = \{(\eta/\xi)[\exp(\xi r) - 1] + 1\}^{-1}. \quad (25)
$$

η and ξ are parameters that depend on N and Z.

In principle, the potentials at the atomic centers in the molecule differ from those of the isolated atoms. However, as demonstrated in [35], good agreement can be obtained with realistic molecular calculations even with the zeroth-order approximation, i.e., using atomic values for η and ξ in Eq. (24).

According to the above discussion, the two-center potential of O_2 is expressed as

$$
V_{\text{mod}}(\mathbf{r}) = V_O^{\text{GSZ}}(r_{O_1}) + V_O^{\text{GSZ}}(r_{O_2}). \quad (26)
$$

$V^{\text{GSZ}}(r)$ can be written as a sum of long- and short-range potentials:

$$
V^{\text{GSZ}}(r) = \frac{Z - (N-1)}{r} + \frac{(N-1)}{r} \Omega(r, \eta, \xi). \quad (27)
$$

For a neutral O atom, $Z = 8$, and $N = 9$. In this case, the long-range part in Eq. (27) disappears, as expected for a neutral atom. As a result, the molecular potential (26) also has a short range. The following parameters were used in the calculation of $V_{\text{mod}}(\mathbf{r})$: $\eta = 2.2145$, $\xi = 1.0478$ [38], and bond length $= 2.42$ a.u.

In the same way as in [33], the equations of motion for the *reversed* collision system, $O_2 \to Ps$, are solved here. This approach has the advantage that the considered processes are analogous to those occurring in the collisions of atoms with heavy particles: fragmentation of Ps and the electron
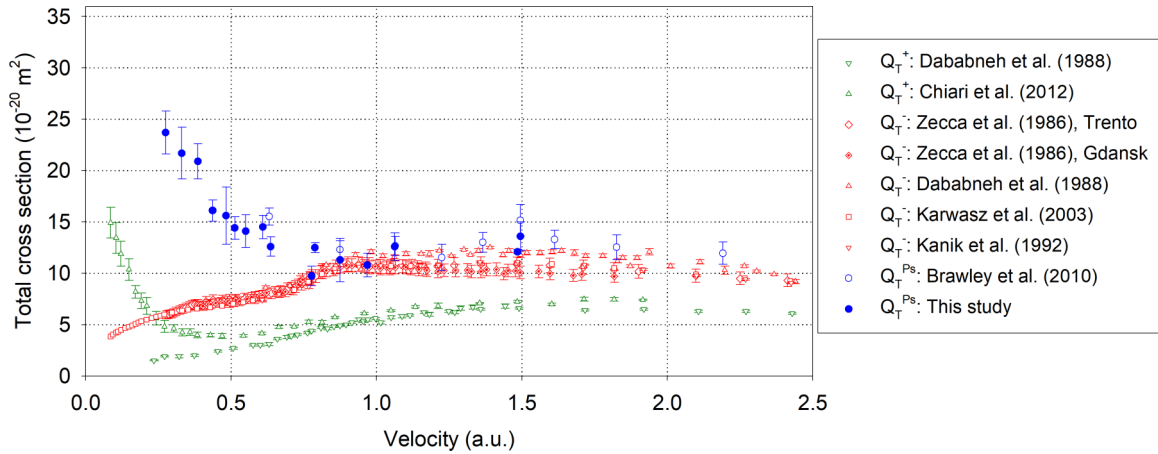
FIG. 2. Experimental Ps-O_2 total cross sections from this study alongside those of Brawley *et al.* [6]. Also shown are equivelocity positron total cross sections of Dababneh *et al.* [41] and Chiari *et al.* [42] and equivelocity electron total cross sections of Zecca *et al.* [43], Dababneh *et al.* [41], Karwasz *et al.* [44], and Kanik *et al.* [45].

transfer between the collision partners correspond to the well-established reaction channels, namely, ionization of the target (free-electron production) and electron capture by the projectile, respectively. In this way, codes that were developed for the description of ion-atom (molecule) collisions can be applied to the present system.

For the random choice of the position and momentum coordinates of the electron, the general procedure proposed by Reinhold and Falcón [39] was followed. The impact parameter of the projectile was chosen randomly in the interval 0–7.5 a.u. The O_2 molecule was also randomly oriented in each collision event. The integration of the equations of motion was started well before the collision (earlier by a time of 350 a.u.). After the collision, a check of the conditions for the exit channels (excitation, ionization, electron capture) was made at a separation of about 100 a.u. For the identification of the capture channel, an O_2 electron-affinity value of 0.01646 a.u. [40] was used. To account fully for the postcollision interaction effects, the integration of the trajectories was continued over distances of 10^8 a.u.

In the present CTMC investigations, the history of 5×10^5 total collision events was followed. After transformation of the calculated trajectories from the reversed system to the direct one, the cross sections for the fragmentation and electron transfer were determined by using the standard procedure of the CTMC:

$$\sigma^{(i)} \approx 2\pi \frac{b_{\max}}{N_{\mathrm{traj}}} \sum_j b_j^{(i)}. \tag{28}$$

Here N_{traj} is the total number of trajectories calculated in the impact parameter range $[0, b_{\max}]$. $b_j^{(i)}$ is the actual impact parameter when the criterion of the regarded reaction channel (fragmentation, electron transfer) is fulfilled.

The results of the calculations are presented and discussed in the next section.

IV. RESULTS AND DISCUSSION

In this work, Q_T^{Ps} has been determined for Ps energies in the range 2–61 eV. The results are shown in Fig. 2 together with

previous measurements [6] and experimental positron (Q_T^+) [41,42] and electron (Q_T^-) [41,43,44] total cross sections at the same velocities. Agreement is noted between the two determinations of Q_T^{Ps} in the common energy range, confirming the electronlike scattering of Ps above approximately 0.8 a.u. However, below this value, a considerable deviation may be observed where the Ps cross section increases with decreasing velocity.

Figure 3 compares Q_T^{Ps} with the sum of the cross sections for elastic scattering and Ps breakup, the dominant inelastic channel, calculated in Ref. [10] using a FEG model and the binary encounter (BE) approximation, respectively. In the present work, the FEG approach has been refined by including (i) the contribution of higher partial waves and, in addition, (ii) the interference term correction to the correlation energy discussed above. The experimental results are seen to be broadly consistent with the trend of the underlying (nonresonant) theoretical cross section, although they are systematically smaller below 30 eV.

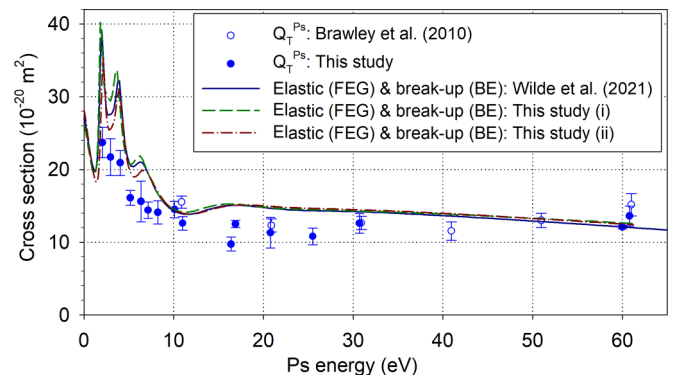The resonance region is considered in more detail in Figs. 4(a) and 4(b). In the former, the measurements are

FIG. 3. Experimental Ps-O_2 total cross sections alongside the sum of the theoretical elastic-scattering (FEG) and breakup (BE) cross sections as presented by Wilde *et al.* [10]. Also shown is the latter with (i) an increased number of higher partial waves and, in addition, (ii) the interference term, as described in the text.
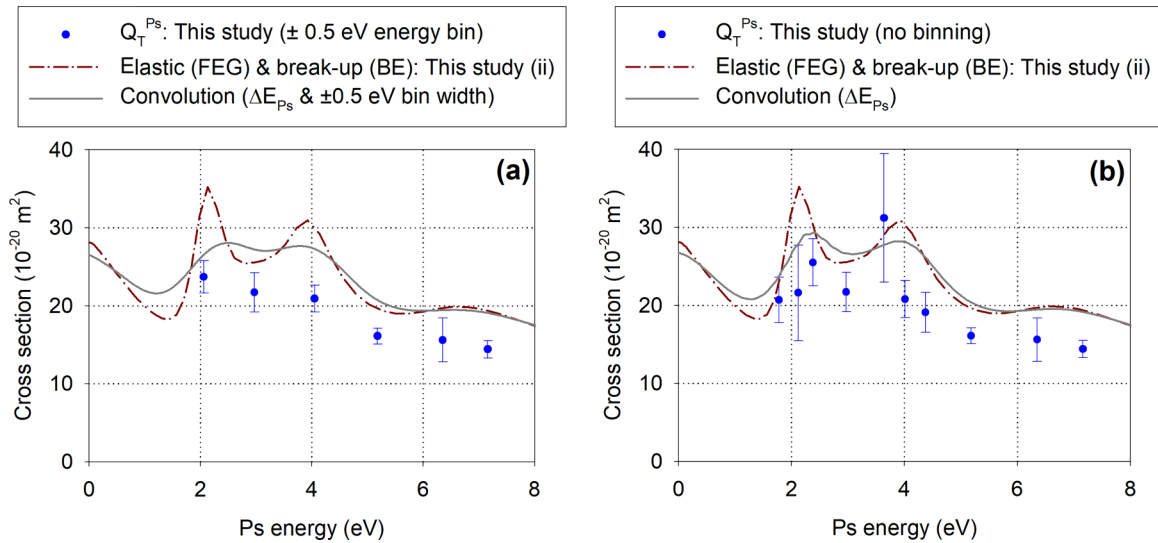
FIG. 4. Experimental Ps-O_2 total cross sections of this study in the energy range 2–8 eV with (a) a 1-eV bin width and (b) no binning. Also shown is the sum of the elastic-scattering (FEG) and breakup (BE) cross sections, labeled curve (ii) in Fig. 3, together with the corresponding convolutions.

compared to the present theory with the interference term [curve (ii) in Fig. 3], and its convolution with the Ps energy distribution ΔE_{Ps} and the (± 0.5 eV) energy bin over which data are combined. To check the sensitivity of the results to the energy grouping, in Fig. 4(b), the means are computed without binning and compared with the same theory convoluted with only the Ps energy distribution. Although suggestive, the resolution and precision of the present results are insufficient to corroborate the predicted resonances. However, once again, both sets of experimental data are systematically lower than theory, suggesting that the elastic-scattering cross section may be overestimated.

The inclusion of the interference correction allows an estimate of the error of the perturbative approach to the correlation potential in the resonance region by considering the corresponding change in amplitude of the peaks ($\simeq 15\%$) and their position ($\simeq 0.3$ eV). However, the major approximation in the theoretical treatment is the use of the local FEG potential for electron exchange. The FEG potential does not prevent capture of the projectile electron into an occupied orbital of the target. To analyze the significance of this approximation for electron-molecule scattering, Morrison and Collins [46] introduced FEG exchange with the orthogonality constraint whereby the continuum orbital is forced to be orthogonal to the occupied orbitals of the target molecule. Still, it is not clear how to employ this method for Ps-molecule collisions since in this case the projectile electron is bound in Ps. Mitroy *et al.* [47,48] proposed the method of the orthogonalized pseudopotential, which reduces the overlap between the wave functions of the projectile and target electrons by introducing a nonlocal potential with a strong repulsive core. This method was successful when applied to Ps scattering by rare-gas atoms [11]. However, it was not able to give a proper description of Ps-molecule scattering [10].

In the absence of a reliable method for incorporating orthogonality constraints in Ps-molecule scattering, the results of Morrison and Collins [46] for electron-molecule scattering

were analyzed. For several molecular targets treated by them (H_2, N_2, CO, and a few polar molecules) the orthogonality constraint substantially improves the FEG results, making them close to those obtained with the exact treatment of exchange. In the low-energy region between $\simeq 0$ and 3 eV, the cross section is reduced by 20%–40%, and the shape resonance position in the case of N_2 and CO is shifted towards lower energy (by about 0.75 eV to $E = 3.54$ eV for CO). The orthogonality constraint becomes less important at higher energies. Thus, it may be reasonably estimated that the error due to the local FEG potential is about the same in Ps-molecule scattering, meaning that the cross sections calculated with the FEG potential overestimate the actual cross sections by about 20%–40% in the energy region below about 5 eV, which is consistent with the experimental values.

A comparison of Q_T^{Ps} with theoretical partial cross sections for elastic scattering, Ps breakup, and O_2^- formation (breakup and electron transfer) is presented in Fig. 5. There the cross sections for elastic scattering are the result of the FEG approach of Wilde *et al.* [10] and its extension [labeled (ii) in this study]. Those for Ps breakup have been computed using both the BE approximation [10] and the present CTMC method. The BE model uses quantum scattering cross sections for electron-molecule and positron-molecule interactions; therefore, quantum effects are implicitly incorporated, although the model by itself is semiclassical. Moreover, the BE results for rare-gas atoms [53] agree with fully quantum-mechanical calculations [54]. The present CTMC results exceed the BE cross sections by a factor of 2–3 above 10 eV. This is consistent with those [33] for the CTMC cross sections for Ps breakup by He atom which exceed quantum-mechanical calculations [55] as well as experimental results [56] by a factor of 1.6–2.5. Thus, it may be concluded that the present disagreement between BE and CTMC reflects quantum effects in e^--O_2 and e^+-O_2 scattering.

Additionally, in Fig. 5, the spin-conversion cross sections for inelastic and elastic processes are displayed. The
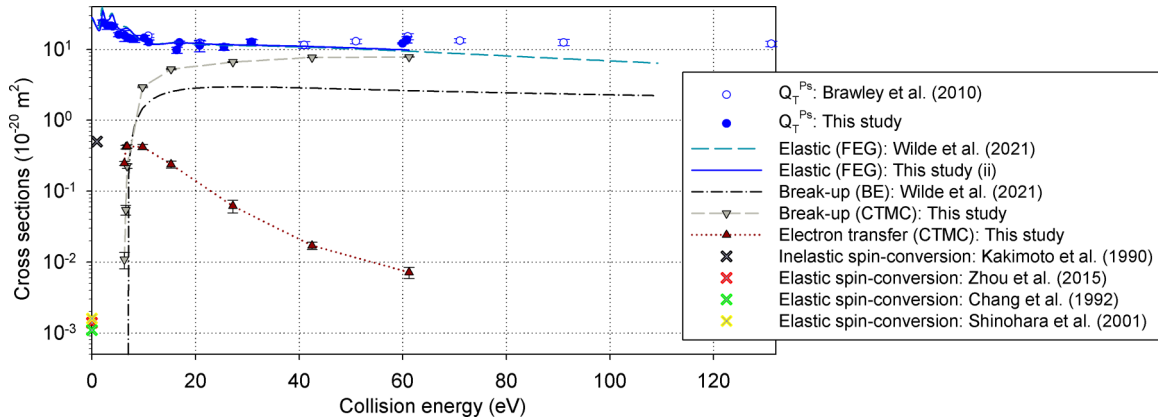
FIG. 5. Experimental Ps-O_2 total cross sections of this study and Brawley *et al.* [6] alongside theoretical partial cross sections: elastic scattering (FEG) of Wilde *et al.* [10] and its extension, this study (ii); breakup (CTMC), this study; electron transfer (CTMC), this study; breakup (BE) of Wilde *et al.* [10]; inelastic spin conversion of Kakimoto *et al.* [49]; and elastic spin conversion of Zhou *et al.* [50], Chang *et al.* [51], and Shinohara *et al.* [52].

cross sections were obtained using the 2γ angular correlation method [49], positron annihilation lifetime spectroscopy, and coincidence Doppler broadening spectroscopy [50–52]. Notably, that for inelastic conversion is several orders of magnitude larger than that for elastic conversion but over a factor of 50 smaller than that for elastic scattering.

V. CONCLUSIONS AND OUTLOOK

The experimental total cross section of positronium scattering from molecular oxygen was presented in the velocity range 0.27–1.50 a.u. (energy range of 2–61 eV) and found to confirm the similarity to the equivelocity electron cross section above 0.87 a.u. (20 eV). However, below this value, the Ps cross section was observed to exceed that for electrons by up to a factor of 4 at the lowest energy. The measurements were compared with the present FEG elastic-scattering cross section, and the two sets of results were found to be consistent within their combined uncertainties. Additionally, cross sections for positronium breakup and O_2^- formation were calculated using a classical-trajectory Monte Carlo approach.

At its peak, the latter is predicted to be $\simeq 35$ times less likely than elastic scattering. It is hoped that in the future measurements with higher-energy resolution and precision will be accompanied by further refinements in concomitant theoretical descriptions.

The data that support the findings of this study are openly available at UCL Discovery [57].

[1] M. Charlton and J. W. Humberston, *Positron Physics*, Cambridge Monographs on Atomic, Molecular and Chemical Physics Vol. 11 (Cambridge University Press, Cambridge, 2001).

[2] D. B. Cassidy, Eur. Phys. J. D **72**, 53 (2018).

[3] S. G. Karshenboim, Phys. Rep. **422**, 1 (2005).

[4] G. Laricchia and H. R. J. Walters, Riv. Nuovo Cimento **35**, 305 (2012).

[5] R. S. Wilde and I. I. Fabrikant, J. Phys. B **53**, 185202 (2020).

[6] S. J. Brawley, S. Armitage, J. Beale, D. E. Leslie, A. I. Williams, and G. Laricchia, Science **330**, 789 (2010).

[7] S. J. Brawley, A. I. Williams, M. Shipman, and G. Laricchia, Phys. Rev. Lett. **105**, 263401 (2010).

[8] M. Shipman, S. J. Brawley, L. Sarkadi, and G. Laricchia, Phys. Rev. A **95**, 032704 (2017).

[9] R. S. Wilde and I. I. Fabrikant, Phys. Rev. A **97**, 052708 (2018).

[10] R. S. Wilde, H. B. Ambalampitiya, and I. I. Fabrikant, Phys. Rev. A **104**, 012810 (2021).

[11] R. S. Wilde and I. I. Fabrikant, Phys. Rev. A **98**, 042703 (2018).

[12] R. S. Wilde, M. K. Selvage, and I. I. Fabrikant, Phys. Rev. A **106**, 032810 (2022).

[13] R. S. Wilde and I. I. Fabrikant, Phys. Rev. A **92**, 032708 (2015).

[14] C. J. Noble and P. G. Burke, Phys. Rev. Lett. **68**, 2011 (1992).

[15] K. Higgins, C. J. Noble, and P. G. Burke, J. Phys. B **27**, 3203 (1994).

[16] J. E. Land and W. Raith, Phys. Rev. A **9**, 1592 (1974).

[17] M. Allan, J. Phys. B **28**, 5163 (1995).

[18] D. M. Newson, M. Shipman, S. J. Brawley, R. Kadokura, T. J. Babij, D. Cooke, D. E. Leslie, and G. Laricchia, J. Instrum. **17**, P11026 (2022).

[19] S. E. Fayer, D. M. Newson, S. J. Brawley, A. Loreti, R. Kadokura, T. J. Babij, J. Lis, M. Shipman, and G. Laricchia, Phys. Rev. A **100**, 062709 (2019).

[20] A. W. Alrowaily, S. J. Ward, and P. Van Reeth, J. Phys. B **52**, 205201 (2019).

[21] A. W. Alrowaily, S. J. Ward, and P. V. Reeth, Atoms **9**, 56 (2021).

[22] I. I. Fabrikant and R. S. Wilde, Phys. Rev. A **97**, 052707 (2018).

[23] A. Özen, A. J. Garner, and G. Laricchia, Nucl. Instrum. Methods Phys. Res., Sect. B **171**, 172 (2000).

[24] M. Shipman, S. J. Brawley, L. Sarkadi, and G. Laricchia, Eur. Phys. J. D **68**, 75 (2014).

[25] M. Shipman, S. Armitage, J. Beale, S. J. Brawley, S. E. Fayer, A. J. Garner, D. E. Leslie, P. Van Reeth, and G. Laricchia, Phys. Rev. Lett. **115**, 033401 (2015).

[26] A. J. Garner, A. Özen, and G. Laricchia, Nucl. Instrum. Methods Phys. Res., Sect. B **143**, 155 (1998).

[27] G. Laricchia, S. Armitage, and D. Leslie, Nucl. Instrum. Methods Phys. Res., Sect. B **221**, 60 (2004).

[28] D. M. Newson, Ph.D. thesis, University College London, 2022.

[29] D. M. Newson, S. J. Brawley, M. Shipman, and G. Laricchia (unpublished).

[30] D. G. Green, A. R. Swann, and G. F. Gribakin, Phys. Rev. Lett. **120**, 183402 (2018).

[31] R. Abrines and I. C. Percival, Proc. Phys. Soc. **88**, 861 (1966).

[32] R. E. Olson and A. Salop, Phys. Rev. A **16**, 531 (1977).

[33] L. Sarkadi, Phys. Rev. A **68**, 032706 (2003).

[34] L. Sarkadi, Phys. Rev. A **92**, 062704 (2015).

[35] S. T. S. Kovács, P. Herczku, Z. Juhász, L. Sarkadi, L. Gulyás, and B. Sulik, Phys. Rev. A **94**, 012704 (2016).

[36] L. Sarkadi, J. Phys. B **49**, 185203 (2016).

[37] A. E. S. Green, D. L. Sellin, and A. S. Zachor, Phys. Rev. **184**, 1 (1969).

[38] R. H. Garvey, C. H. Jackman, and A. E. S. Green, Phys. Rev. A **12**, 1144 (1975).

[39] C. O. Reinhold and C. A. Falcón, Phys. Rev. A **33**, 3859 (1986).

[40] K. M. Erwin, I. Anusiewicz, P. Skurski, J. Simons, and W. Carl Lineberger, J. Phys. Chem. A **107**, 8521 (2003).

[41] M. S. Dababneh, Y.-F. Hsieh, W. E. Kauppila, C. K. Kwan, S. J. Smith, T. S. Stein, and M. N. Uddin, Phys. Rev. A **38**, 1207 (1988).

[42] L. Chiari, A. Zecca, S. Girardi, E. Trainotti, G. García, F. Blanco, R. P. McEachran, and M. J. Brunger, J. Phys. B **45**, 215206 (2012).

[43] A. Zecca, R. S. Brusa, R. Grisenti, S. Oss, and C. Szmytkowski, J. Phys. B **19**, 3353 (1986).

[44] G. P. Karwasz, R. S. Brusa, and A. Zecca, *Interactions of Photons and Electrons with Molecules* (Springer-Verlag, 2003).

[45] I. Kanik, J. C. Nickel, and S. Trajmar, J. Phys. B **25**, 2189 (1992).

[46] M. A. Morrison and L. A. Collins, Phys. Rev. A **23**, 127 (1981).

[47] J. Mitroy and G. G. Ryzhikh, Comput. Phys. Commun. **123**, 103 (1999).

[48] I. A. Ivanov, M. W. J. Bromley, and J. Mitroy, Comput. Phys. Commun. **152**, 9 (2003).

[49] M. Kakimoto, T. Hyodo, and T. B. Chang, J. Phys. B **23**, 589 (1990).

[50] Y. Zhou, W. Mao, Q. Li, J. Wang, and C. He, Chem. Phys. **459**, 81 (2015).

[51] T. Chang, G. Yang, and T. Hyodo, Mater. Sci. Forum **105–110**, 1509 (1992).

[52] N. Shinohara, N. Suzuki, T. Chang, and T. Hyodo, Phys. Rev. A **64**, 042702 (2001).

[53] G. F. Gribakin, A. R. Swann, R. S. Wilde, and I. I. Fabrikant, J. Phys. B **49**, 064004 (2016).

[54] C. Starrett, M. T. McAlinden, and H. R. J. Walters, Phys. Rev. A **72**, 012508 (2005).

[55] J. E. Blackwood, C. P. Campbell, M. T. McAlinden, and H. R. J. Walters, Phys. Rev. A **60**, 4454 (1999).

[56] S. Armitage, D. E. Leslie, A. J. Garner, and G. Laricchia, Phys. Rev. Lett. **89**, 173402 (2002).

[57] https://discovery.ucl.ac.uk/id/eprint/10164844/.